Large-Scale Variations in Ozone from the First Two Years of *UARS* MLS Data

LEE S. ELSON, GLORIA L. MANNEY, LUCIEN FROIDEVAUX, AND JOE W. WATERS

Jet Propulsion Laboratory, California Institute of Technology, Pasadena, California

(Manuscript received 15 March 1994, in final form 13 July 1994)

ABSTRACT

Two years of stratospheric measurements of ozone from the *Upper Atmosphere Research Satellite* Microwave Limb Sounder are examined in order to characterize large horizontal scale wave variations. The use of Fourier analysis allows the detection of variations from daily through seasonal and interannual timescales. High-latitude winter variations at 10 hPa often have very large amplitudes, but smaller midlatitude variations are more ubiquitous. Some variations have the characteristics of locally generated instabilities. Correlations of wave features with changes in the zonal-mean ozone at 10 hPa suggest the presence of significant horizontal motions during strong wintertime polar warming events. Such correlations are not evident at other levels. Spectral analysis of the large-scale variations show most waves to be slowly propagating. In contrast to some past observations, equatorial regions are shown to lack large amplitude wave events.

1. Introduction

Planetary-scale waves are known to be important mechanisms for transport processes in the middle atmosphere. There are many indicators of wave activity including temperature and species concentrations. Each of these indicators has been studied in the past for insight into a variety of wave mechanisms. This discussion will focus on an overview of wave variations in ozone concentration as measured during the first two years of operation of the Microwave Limb Sounder (MLS) (Barath et al. 1993) on the *Upper Atmosphere Research Satellite* (*UARS*) (Reber 1990). A companion paper (Froidevaux et al. 1994) traces the evolution of zonal-mean ozone over a similar period.

There are several reasons why the MLS dataset provides a unique view of ozone in the middle atmosphere. Unlike the Total Ozone Mapping Spectrometer (TOMS) its vertical measurement resolution (about 4 km) allows the inspection of vertical variations within the ozone column. Although MLS retrievals occur at levels separated by about 5 km, vertical resolution is superior to *Nimbus-7* Solar Backscatter Ultraviolet (SBUV) measurements, which have Gaussian-shaped averaging kernels 8–10 km in width (Randel and Gille 1991). In addition, unlike SBUV and TOMS, MLS is able to detect ozone during the night. The length of the MLS data record is shorter than SBUV and TOMS, so interannual variations are not as well represented in the MLS data. As described by Gille and Russell (1984), the Limb Infrared Monitor of the Stratosphere (LIMS) on *Nimbus-7* had capabilities similar to MLS but provided data only for about 8 months. In addition, LIMS was unable to view latitudes south of about −64°. Although MLS is able to view latitudes as far south as −80°, it cannot do so all of the time. Because *UARS* performs a yaw maneuver approximately every 36 days (one *UARS* "month"), MLS alternately views latitudes from about −34° to 80° and from 34° to −80°. Although the middle and high latitudes are undersampled by this viewing procedure, the low latitudes (±34°) are sampled continuously, except for data outages.

One area of focus in past studies has been that of ozone variability on seasonal to interannual timescales. Perliski and London (1989) examined 9 years of SBUV data. Among their findings was that longitudinal wavenumber 1 variations had largest amplitudes in the polar regions with a secondary maximum over the equator. Randel (1993) also analyzed SBUV data and found evidence that planetary wave events associated with polar warmings can influence zonal-mean ozone over nearly the entire globe. It must be noted, however, that according to Randel and Gille (1991) SBUV data may underestimate wave amplitudes by 20%–60% depending on the vertical structure of the disturbance.

Planetary-scale waves have been examined on shorter timescales as well. Kelvin waves hold a great deal of interest because they serve to transport momentum and chemical species in the Tropics. Salby et al. (1990) and Randel (1990) examined ozone power spectra from LIMS observations and found a clear Kelvin wave signature (eastward propagating wave 1 and 2 variations with periods ranging from about 4 to 40 days). Canziani et al. (1994) provide a similar study

Corresponding author address: Dr. Lee S. Elson, M/S 183-701, Jet Propulsion Laboratory, 4800 Oak Grove Drive, Pasadena, CA 91109.

using MLS data. Their discussion of ozone variations associated with Kelvin waves focuses on two time periods near the solstices during the first *UARS* year. They found similarities with the earlier LIMS studies but also some differences, including a greater amount of asymmetry about the equator. Kelvin wave amplitudes in ozone concentration are typically at least an order of magnitude smaller than other variations and are therefore not evident in the figures discussed here.

LIMS observations have also been used to investigate another important source of planetary waves: instability. It is well known that unstable disturbances are generated near the equatorial and polar flanks of the polar night wind jet. For example, Elson (1990) found that during the winter months in 1979, an unstable mode centered near 20° and 10 hPa was evident in the ozone field. The small vertical scale (about 10 km) of this type of feature would make it hard to properly measure in SBUV data. This instability traveled westward with a period near 13 days.

The purpose of the discussion here is to provide an overview of planetary-scale ozone variations as measured by MLS from October 1991 through September 1993. Section 2 will describe the method used to analyze the data. Section 3 will present an overview of wave activity at several pressure levels for each of the two years. In addition, several limited time periods will be examined in greater detail. Comparisons will be made between the time evolution in the zonal-mean, wavenumber 1, and wavenumber 2 ozone. Section 3 will also examine the variance spectra for midlatitude disturbances and will provide examples of the vertical structure of these disturbances. Comparisons will be made with earlier studies.

2. Data analysis: Fourier transforms

Elson and Froidevaux (1993, hereafter EF) have described the production of synoptic MLS maps. The approach begins with a coordinate system rotation in order to calculate Fourier transforms of the time and longitude dependence of ozone concentration. This technique, described by Salby (1982a,b), makes use of fast Fourier transforms at selected latitudes and heights to produce Fourier transform coefficients for discrete values of m, the longitudinal wavenumber, and σ, the frequency. The input series must be equally spaced in longitude and time, a requirement made more difficult by the variability of the *UARS* orbital period. This variability is small enough to allow the routine calculation of Fourier coefficients over a 7.2-day (108 orbit) period, and unless otherwise indicated, these coefficients are used here. Longer calculations (e.g., over a *UARS* month) are possible only during times when the orbital period is very slowly changing. As discussed by Elson (1990), there is a trade-off between better frequency resolution and interference caused by transience as one increases the sample length. The 60-day sample lengths, found useful for analyzing LIMS data, are not possible using the present approach unless a remapping (e.g., Canziani et al. 1994) is carried out. Nevertheless, the frequency resolution obtained here for several cases with sample lengths of order 30 days is quite adequate.

The Fourier transform coefficients are used here in two different ways. In order to demonstrate the variability of ozone on seasonal to interannual timescales, all resolved frequency contributions to the inverse transform for individual zonal harmonics (including the zonal mean) are displayed at several pressure levels as a function of time. We refer to this as "zonally averaged fluctuations" or "wavenumber 1 fluctuations." The sine and cosine components are also used to calculate the cross-spectral and power spectral density functions, as described by Bendat and Piersol (1971). These functions are then spectrally smoothed using a Hanning window. This smoothing is necessary, in part, in order to provide reasonable estimates of statistical significance. Such estimates are found by calculating coherency and relating it to a posteriori probability (Elson 1990). The spectral density functions are also used to find the eastward and westward propagating wave variances described by Schäfer (1979). As discussed by EF, the Fourier series corresponding to the ascending and descending parts of the orbit cease to be independent as one approaches the turning points of the orbit. This can produce artifacts in the form of scalloping effects poleward of ±75°.

3. Results

a. Time evolution of wavenumber components

The zonally averaged ($m = 0$) fluctuations of ozone concentration during the first two years of observations show several interesting features, as discussed by Froidevaux et al. (1994). The absolute value of wavenumber 1 ($m = 1$) fluctuations at pressure levels of 46, 10, and 2 hPa (*UARS* levels 8, 12, and 16) is shown here in Fig. 1. Missing days (e.g., *UARS* yaw maneuvers, field-of-view contamination from the moon, platform and instrument problems) have been omitted, resulting in gaps in this and similar figures. Wave activity is seen to be transient in nature but predominant during the fall, winter, and spring months in each hemisphere and at all levels shown. Of the three levels, 10 hPa exhibits the largest amplitude. Interannual variability can also be seen at all levels, with a very large difference occurring near 60° at 10 hPa during December and January (*UARS* days 84–124 and 446–485). Note that *UARS* began its operation on 12 September 1991 (*UARS* day 1).

The results for $m = 2$ fluctuations are similar in structure to those for $m = 1$ but the amplitudes are generally smaller. Figure 2 shows these amplitudes at the same levels as Fig. 1. Although both wave 1 and wave 2 are usually present during the active months, there are

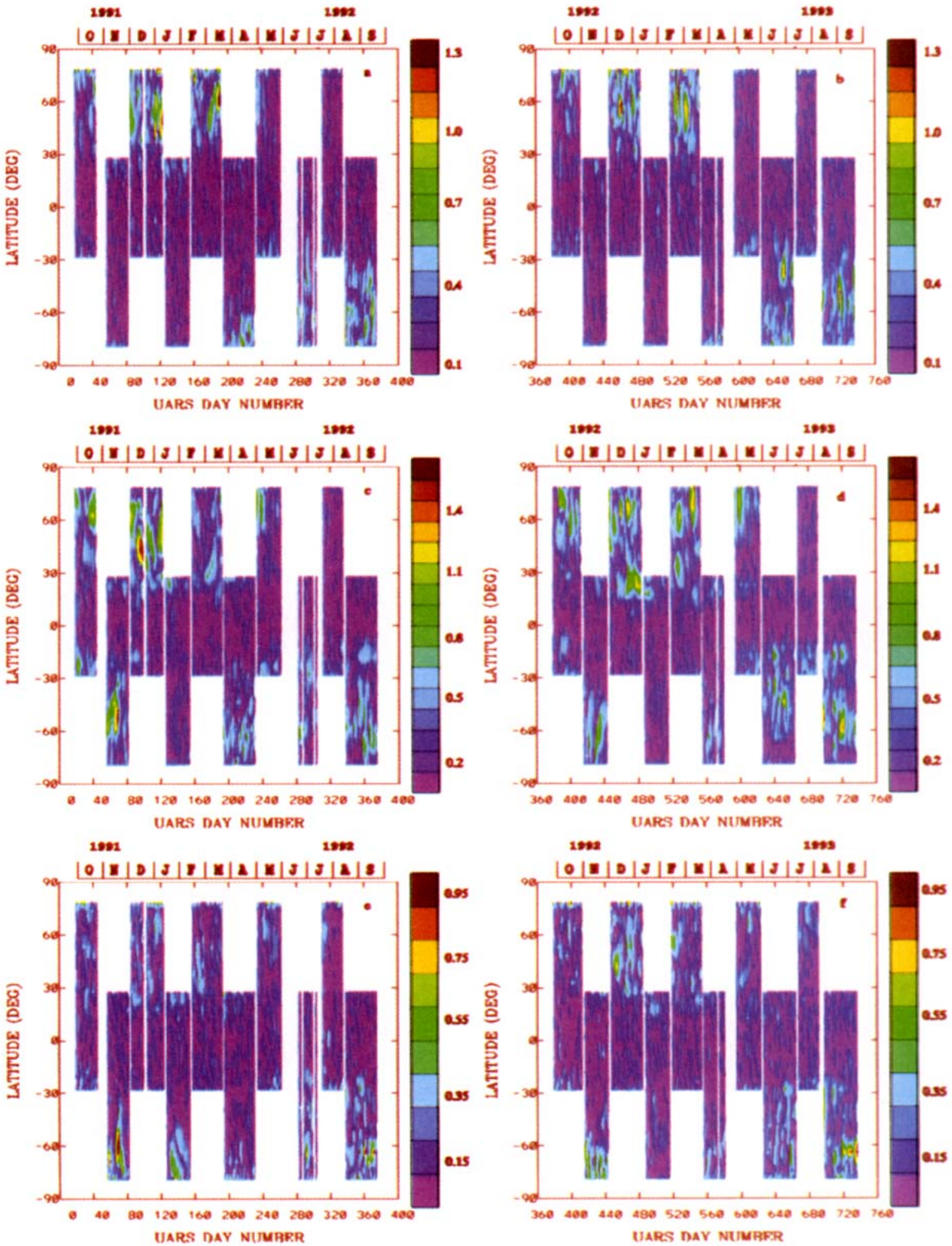

FIG. 1. Time evolution of the amplitude of wave 1 ozone fluctuations (ppmv) at (a) 2 hPa for *UARS* days 20–375, (b) 2 hPa for *UARS* days 380–736, (c) 10 hPa for *UARS* days 20–375, (d) 10 hPa for *UARS* days 380–736, (e) 46 hPa for *UARS* days 20–375, and (f) 46 hPa for *UARS* days 380–736.

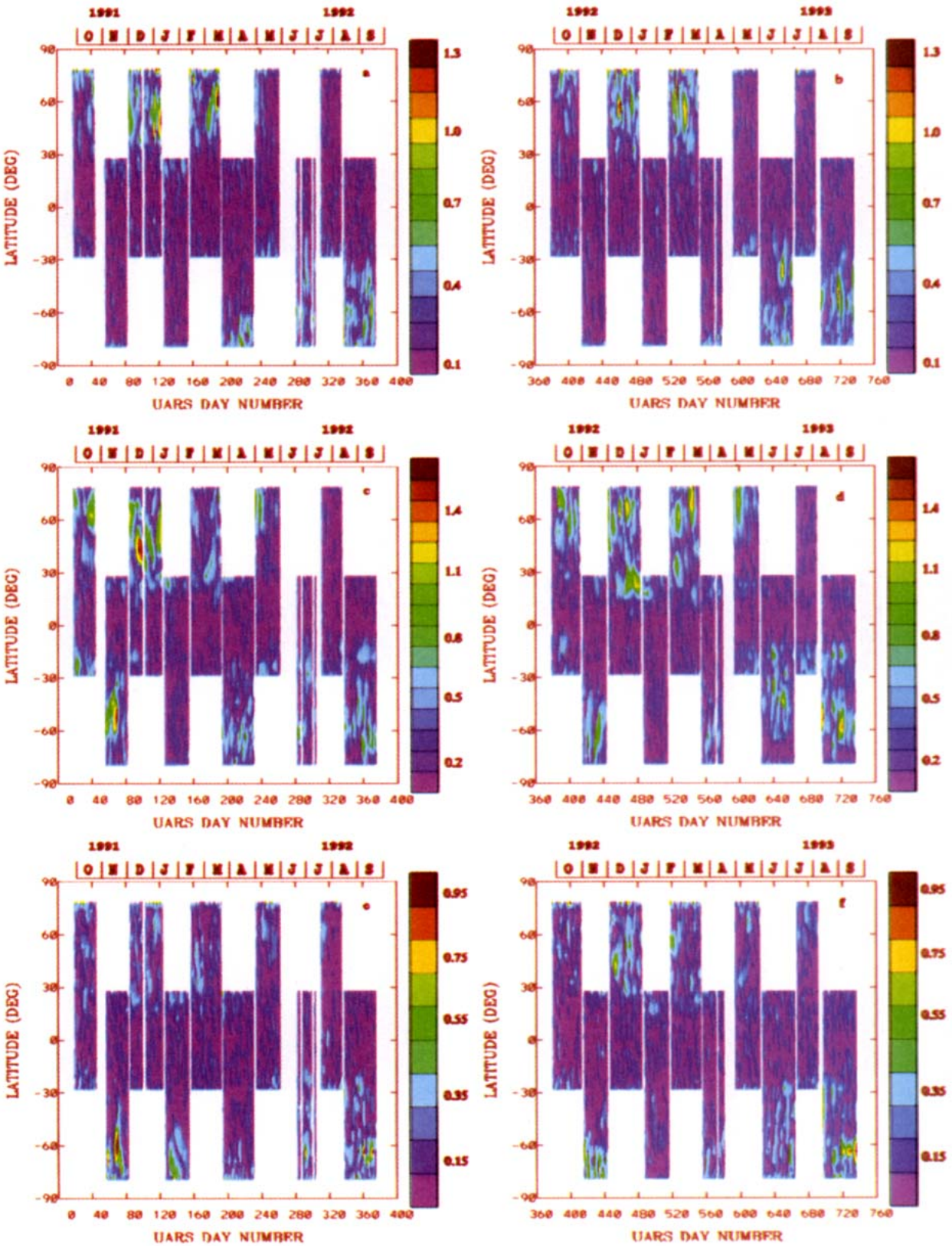

FIG. 2. Same as Fig. 1 but for wave 2 ozone fluctuations.

some noteworthy departures from this pattern. Days 54–83 (November 1991) show the southern midlatitudes to be quite active with wave 2 events, but nearly devoid of wave 1 at 10 hPa. Similarly, days 626–665 (June 1993) contain significant levels of wave 1 activity but little wave 2 activity in this same latitude region at 46 hPa. Manney et al. (1991a) found comparable behavior when they examined the height field from National Meteorological Center (NMC) data.

Closer inspection of Fig. 1 yields several interesting features. In both hemispheres, wave activity appears to be strongest, especially at 10 hPa, in two somewhat distinct bands: one between 60° and 80° and a second, smaller one in the 20°–35° range. The equatorial region seems particularly devoid of large amplitudes. These findings are in marked contrast to the equatorial SBUV results of Perliski and London (1989) described above but are quite similar to the LIMS results described by Elson (1990).

Figures 1 and 2 lead to the question of whether the time and latitude structure of the wave events can be linked to a mechanism. As discussed above, one possibility is locally generated instabilities. The latitude gradient of potential vorticity (PV) can provide an indicator of the likelihood of instability, at least in the small amplitude approximation (Manney et al. 1988). Figure 3 shows this quantity on the 840-K potential temperature surface (near 10 hPa), derived from U.K. Meteorological Office data using the technique described by Manney and Zurek (1993), for the two years shown in Figs. 1 and 2. The white contours show zero values of the PV gradient, that is, the region where the necessary condition for instability is satisfied. The temporal correlation with large wave events at high latitudes in both hemispheres is stronger during the spring months. This is consistent, at least in the Southern Hemisphere, with past suggestions (Manney et al. 1991b) that instability in the polar regions is most important during the spring breakup of the vortex. According to the results of Manney et al. (1991a), there is considerable interannual variability in the location and timing of sign changes in PV. This is reflected in Fig. 3 where the area bounded by white contours in October is much greater in 1992 than 1991. In Fig. 4, we focus on a late winter period (days 518–554) in the Northern Hemisphere. This figure shows the PV gradient and the amplitude of wave 2 fluctuations. Wave 2 is often the fastest growing mode for an unstable basic state (Elson 1990; Manney et al. 1991b). The most extensive region bounded by zero gradient values corresponds in time and latitude to the largest $m = 2$ amplitude poleward of 60° between days 541 and 550. Although this structure is similar to that found by Manney et al. (1991a) for height fields in the Southern Hemisphere, a more definitive identification of mechanisms requires an examination of the height and temperature fields for this time period. As discussed by Elson (1990), the spatial structure of unstable disturbances in ozone and temperature can be quite different.

By expanding the time axes in Fig. 1 and comparing $m = 0$ and $m = 1$ amplitudes, one can see significant differences with altitude in how the waves and the zonal mean interact. Several periods with large wave amplitudes have been selected for discussion. Figures 5a

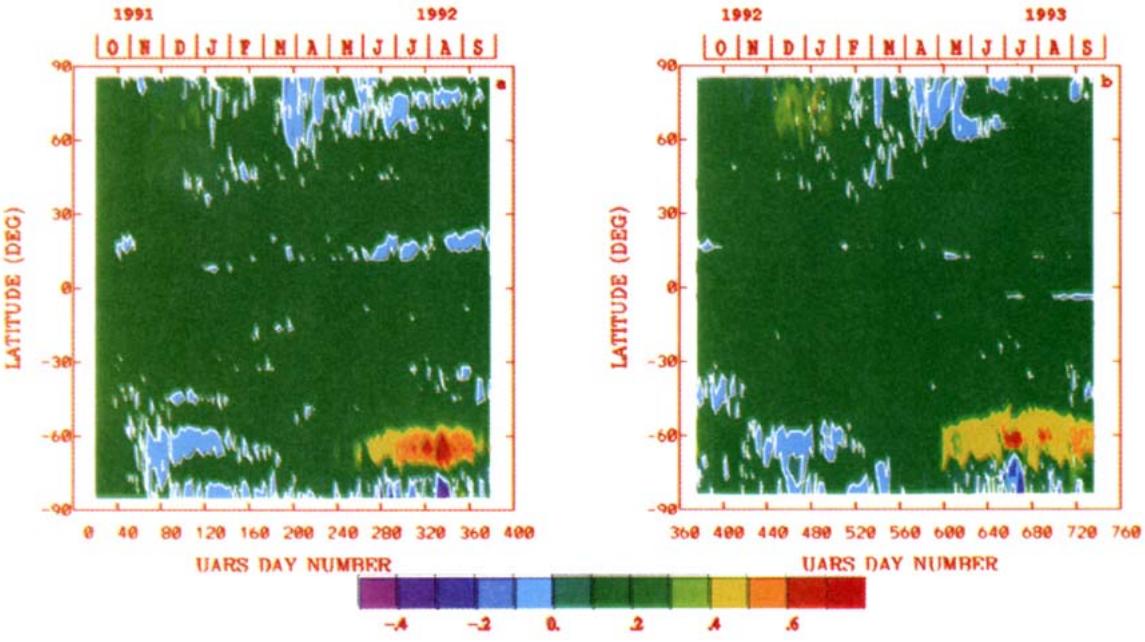

FIG. 3. Potential vorticity gradient (10^{-4} km^2 kg^{-1} s^{-1} deg^{-1}) on an 840-K potential temperature surface for (a) the first *UARS* year (days 20–375) and (b) the second *UARS* year (days 380–736). The zero value is highlighted by a white contour.

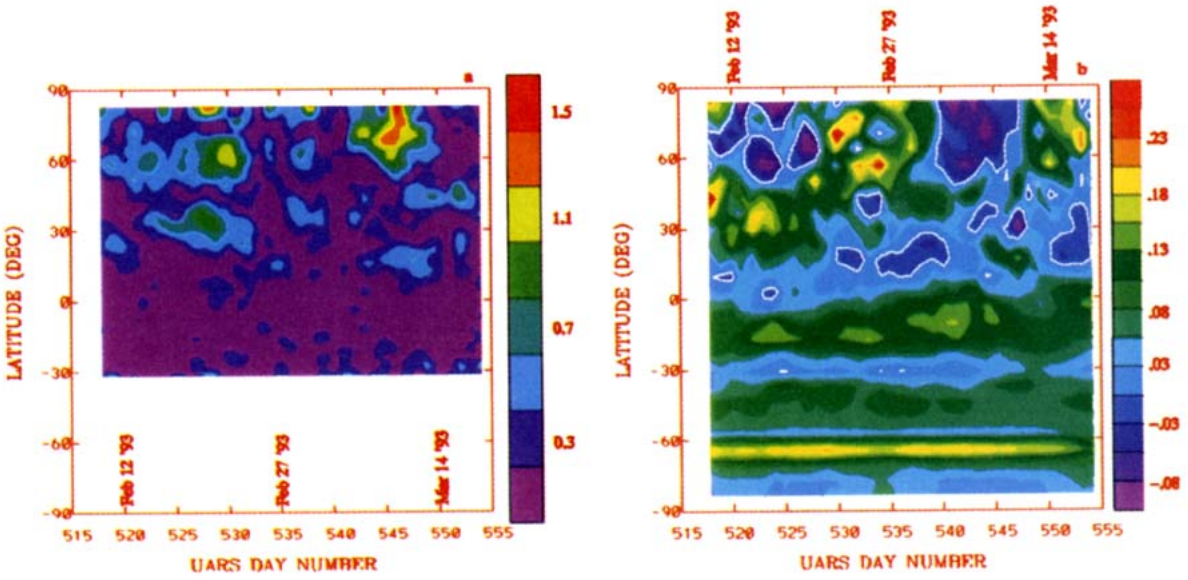

FIG. 4. (a) Amplitude of wave 2 ozone fluctuations (ppmv) versus time for *UARS* days 518–554 (10 Feb 1993–18 Mar 1993) at 10 hPa and (b) potential vorticity gradient on an 840-K potential temperature surface (10^{-4} km^2 kg^{-1} s^{-1} deg^{-1}) for the same period. The zero value is highlighted by a white contour.

and 5b show the $m = 0$ and $m = 1$ amplitude fluctuations for February and March 1993 at 2 hPa. At these levels, there does not seem to be much temporal correlation between changes in zonal-mean ozone and wave 1 amplitude. This behavior is typical for the 2-hPa data examined here and is in disagreement with the findings of Randel (1993) based on SBUV data from 1979 to 1981.

At 10 hPa in August and September of 1992 (Figs. 5c and 5d) the situation is quite different. Here we see that not only are the wave 1 amplitudes larger, but there is a definite signature in the zonal mean that corresponds in time and latitude to the large amplitude, transient wave events near days 361 and 371. These warming events were described by Fishbein et al. (1993) who noted their approximate 9-day periodicity. The time evolution of the zonal-mean concentration implies that there is at least temporary poleward transport of ozone during the buildup of the wave 1 event. This type of correlation is not uncommon at 10 hPa and always has similar characteristics. Evidence that horizontal ozone transport is important at 10 hPa is to be expected since the concentration peaks near this level, making transport by vertical motions less likely.

At 46 hPa, during the northern winter of 1991, large wave 1 amplitudes appear in the same latitude band as the large time tendencies in the zonal mean, as shown in Figs. 5e and 5f. The time correlation between the two, however, is not obvious. As is the case at 2 hPa, the mean ozone concentration near 60° shows evidence of changes by the creation or deletion of closed contours, as would be the result of vertical transport. This is in contrast to the behavior at 10 hPa (Fig. 5c) where mean changes result from bending of existing contours as would be the case with horizontal transport. Much of the structure at 46 hPa is likely to be determined by the position and dynamics of the polar vortex.

b. Spectral analysis and spatial structure of selected features

The wave 1 and 2 ozone variations described above have distinctive vertical structure as well as preferred frequencies. Fishbein et al. (1993) characterized warming events during an active period in the Southern Hemisphere. Here, we describe a more quiescent period, when MLS was looking south. For the period chosen, 10 January–8 February 1993 (*UARS* days 487–516), the *UARS* orbital period was quite constant, allowing a 30-day record to be used for spectral analysis. The amplitude of the wave 1 and 2 variance is shown, at several altitudes, in Fig. 6 as a function of latitude and frequency. Several panels in this figure show large amplitudes near the 1-day westward propagating limit of the diagram. These large amplitudes are the result of a small systematic difference in the ascending and descending branches of the MLS data and should be regarded as artificial. Some panels also show significant amplitude very near the polar limit of the data. As discussed above, this is the result of the lack of independence between the ascending and descending datasets in this region. From Fig. 6, it can be seen that there is significant variation of both the latitude structure and propagation characteristics with altitude. In general, the spectra are peaked at the smaller frequencies (usually referred to as "red") but much of the slow-moving

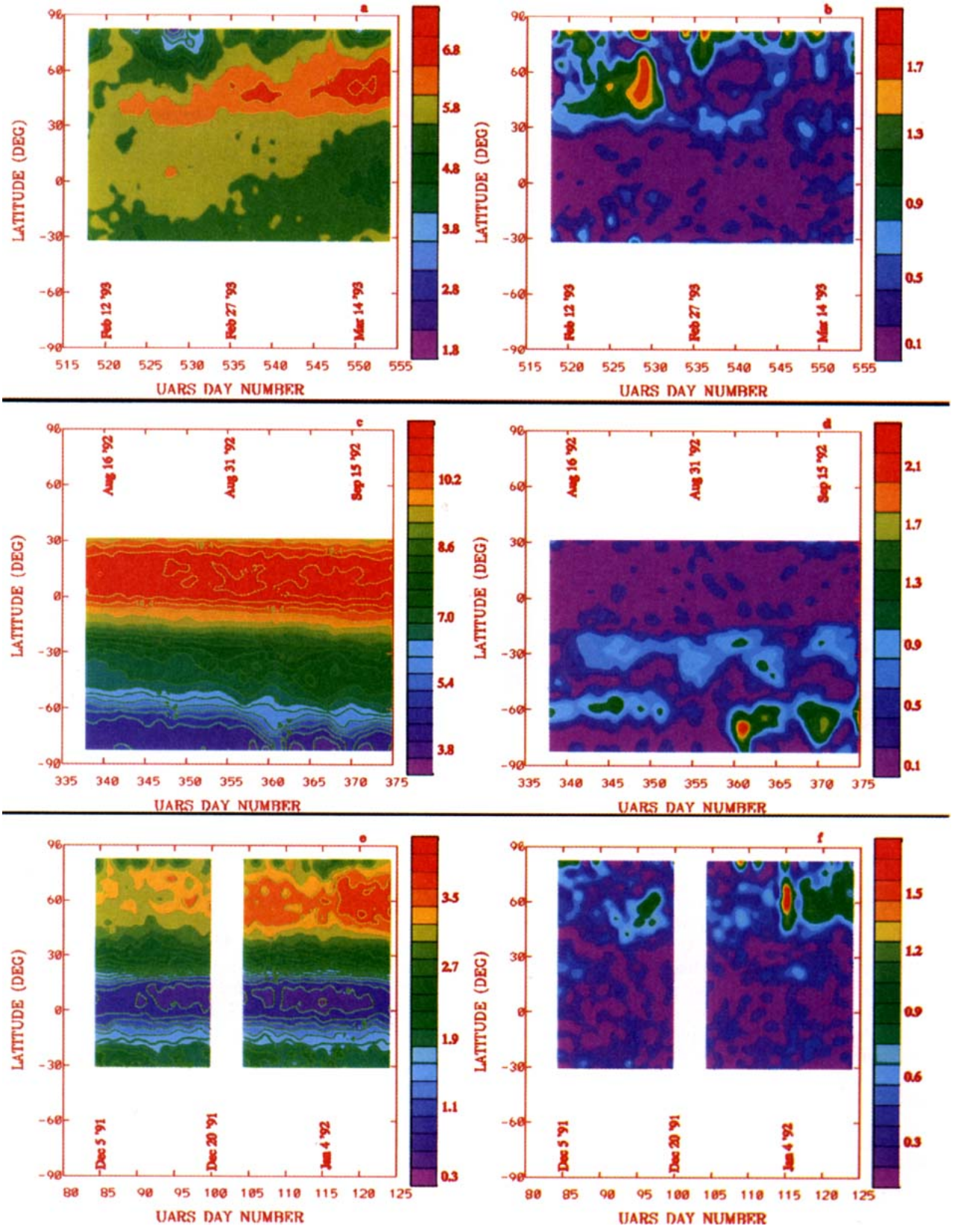

FIG. 5. Zonally averaged [(a), (c), (e)] and wave 1 fluctuations [(b), (d), (f)] of ozone (ppmv) versus time at 2 hPa [(a) and (b)], 10 hPa [(c) and (d)], and 46 hPa [(e) and (f)]. Panels (a) and (b) cover a period in Feb and Mar 1993, (c) and (d) in Aug and Sep 1992, and (e) and (f) in Dec 1991 and Jan 1992.

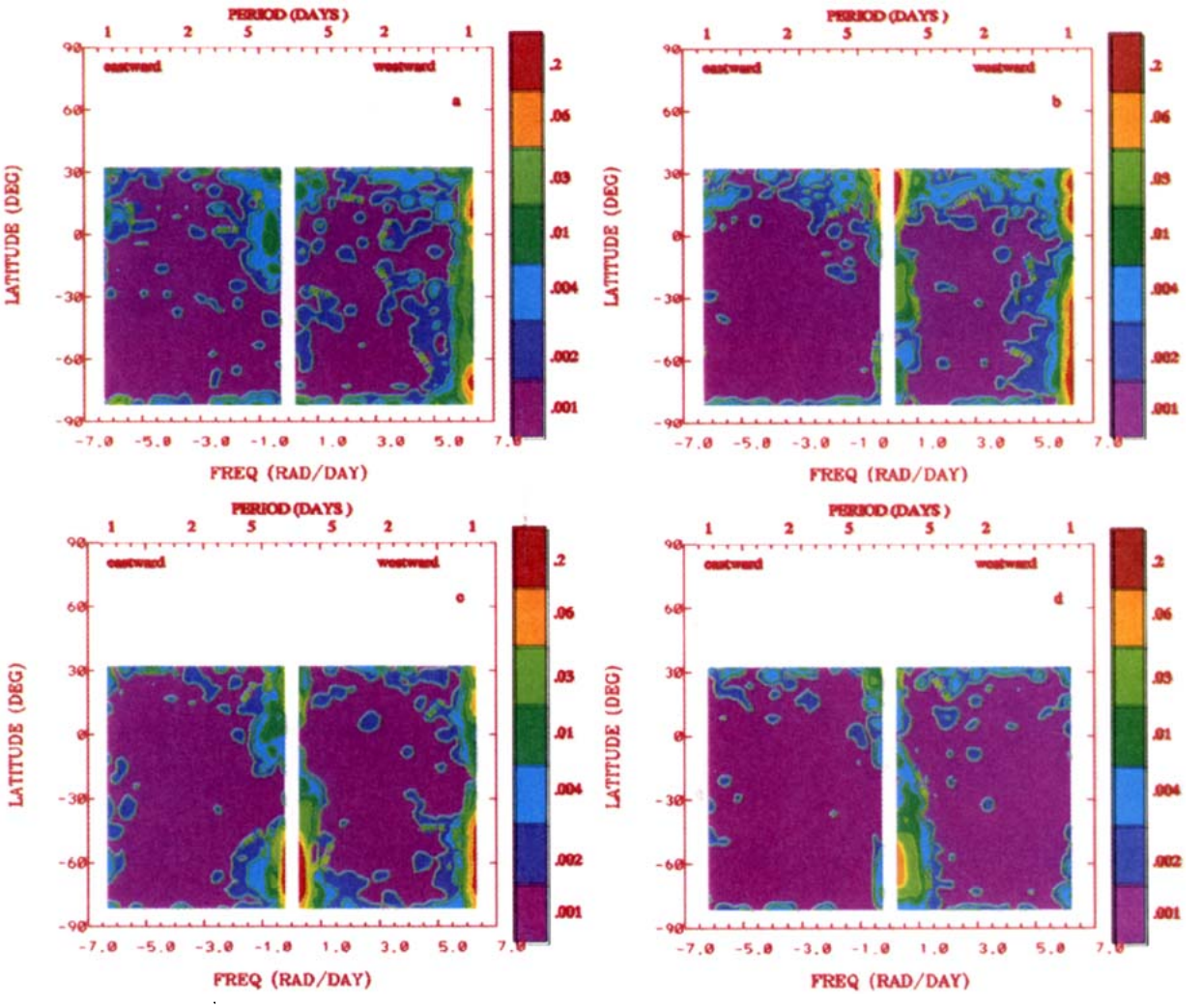

FIG. 6. Wave variance amplitude of ozone (ppmv) at (a) 2 hPa, (b) 10 hPa, and (c) 22 hPa. All panels are for wave 1 except (d), which shows wave 2 at 22 hPa. *UARS* days 487–516 are covered. Color and contour scales are logarithmic.

variance changes from eastward to westward and back to eastward as one moves from 2 to 10 to 22 hPa. The largest amplitudes occur at 10 hPa and +25° and at 22 hPa and −65°. Wave 2 also has its largest amplitude in this latter region. In addition, there is a relative maximum centered at the equator at 2 and 22 hPa, but not at 10 hPa. Notice that the amplitudes of these equatorial variations are quite small. Although this is due in part to the spectral smoothing, an examination of Fig. 1 shows that all unsmoothed frequencies together do not produce large equatorial fluctuations.

We can examine the latitude and height structure of variance amplitude in a frequency band where that variance is large. Figure 7 shows the height/latitude structure of the variance amplitude in a band centered at a period of 15 days (westward) for this same time in 1993. Two features are evident in both wave 1 and 2, one near +30° and 10 hPa and one near −60° and 20 hPa. Both features are of limited vertical extent with the more poleward feature showing a greater degree of coherency between the cosine and sine components. The midlatitude feature has structure quite similar to that observed in the LIMS data (see Fig. 7 of Elson 1990).

4. Discussion

Large-scale wave fluctuations in the ozone concentration measured by *UARS* MLS show a strong dependence on season, latitude, and altitude as well as interannual variation. Since the measured variations depend on the spatial gradients of the zonal-mean ozone concentration, it is possible to infer qualitative characteristics of transport when these gradients are taken into

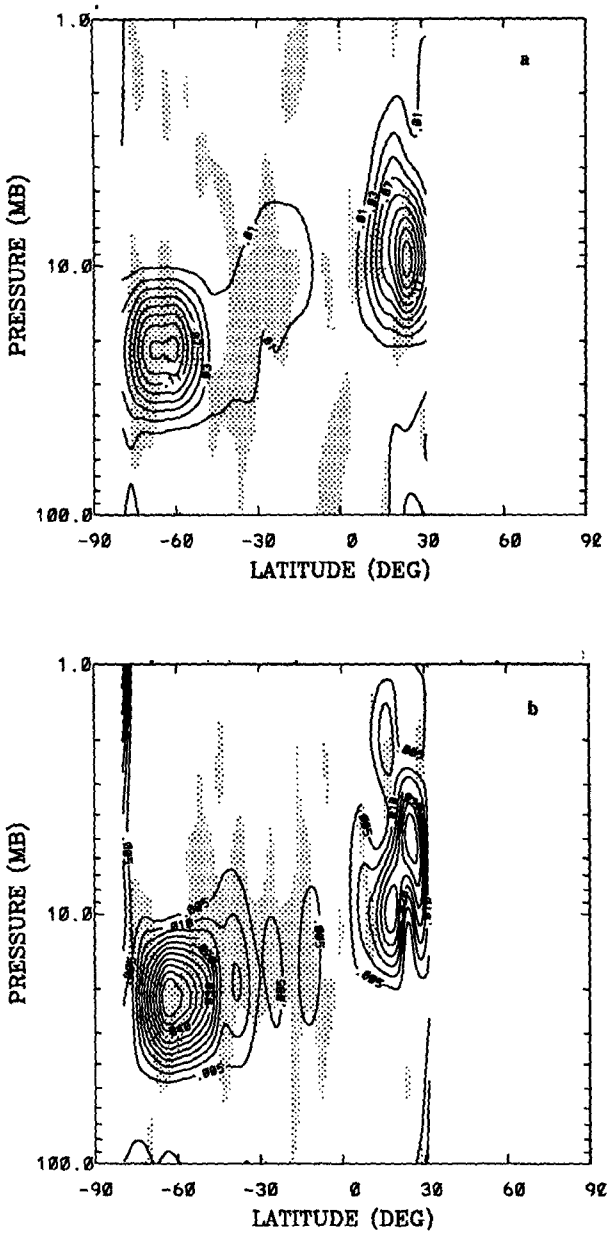

FIG. 7. (a) Wave 1 variance amplitude of ozone (ppmv) versus altitude and latitude for variations with periods between 11.9 and 20.9 days. Shaded region denotes areas where the coherency corresponds to a probability of 90% or more. (b) Same as (a) but for wave 2. *UARS* days 487–516 are covered.

account. Amplitudes are largest in the winter polar regions near 10 hPa where the zonal-mean gradients are large and predominantly horizontal, so horizontal transport is likely to be important. Although not shown, a similar examination of water vapor, which has a different zonal-mean concentration distribution, suggests that vertical contributions to transport are less important here.

Many of the ozone disturbances detected by MLS are of limited vertical extent so that differences with SBUV observations might be expected. For example, the characteristics of SBUV data, which implied strong interactions between waves and the mean ozone concentrations, attributed to the 2-hPa level may have had a contribution from the lower altitudes. It is more difficult to explain differences between SBUV and MLS observations of equatorial variations. The SBUV results of Perliski and London (1989) for a 9-year average showed significantly more amplitude between $\pm 20°$ than for either of the MLS years. Several aspects of their analysis make larger SBUV amplitudes a surprise. Their evaluation examined the mean of monthly averages over the 9-year dataset (1978–87). These averages filtered out traveling wave variations. The MLS results included all resolvable frequencies and examined individual years. Both of these aspects should have exaggerated the MLS results compared to those of the SBUV if the same signal were present in both datasets. Whether this difference represents a real trend or an artifact in one or both datasets remains to be determined. Part of a *UARS* validation effort currently under way involves the comparison of MLS, SBUV, and other *UARS* ozone measurements. Characteristics of the middle-to-high latitude wavenumber 1 results of Perliski and London are similar to those of MLS. Wave amplitudes seem to be large in the Northern Hemisphere during October through February and large in the Southern Hemisphere from July through November.

Acknowledgments. The authors thank the *UARS* project and the MLS team for providing support and the UKMO for supplying data. This research was sponsored by NASA's *Upper Atmosphere Research Satellite* Project and was performed at the Jet Propulsion Laboratory, California Institute of Technology, under contract with the National Aeronautics and Space Administration.

REFERENCES

Barath, F. T., and Collaborators, 1993: The Upper Atmosphere Research Satellite Microwave Limb Sounder Instrument. *J. Geophys. Res.*, **98,** 10 751–10 762.

Bendat, J. S., and A. G. Piersol, 1971: *Random Data: Analysis and Measurement Procedures.* Wiley-Interscience, 407 pp.

Canziani, P. O., J. R. Holton, E. F. Fishbein, L. Froidevaux, and J. W. Waters, 1994: Equatorial Kelvin waves: A *UARS* MLS view. *J. Atmos. Sci.*, **51,** 3053–3076.

Elson, L. S., 1990: Satellite observations of instability in the middle atmosphere. *J. Atmos. Sci.*, **47,** 1065–1074.

——, and L. Froidevaux, 1993: The use of Fourier transforms for asynoptic mapping: Applications to the Upper Atmosphere Research Satellite Microwave Limb Sounder. *J. Geophys. Res.*, **98,** 23 039–23 049.

Fishbein, E. F., L. S. Elson, L. Froidevaux, G. L. Manney, W. G. Read, J. W. Waters, and R. W. Zurek, 1993: MLS observations of stratospheric waves in temperature and ozone during the 1992 southern winter. *Geophys. Res. Lett.*, **20,** 1255–1258.

Froidevaux, L., J. W. Waters, W. G. Read, L. S. Elson, D. A. Flower, and R. F. Jarnot, 1994: Global ozone observations from *UARS*

Microwave Limb Sounder: An overview of zonal-mean results. *J. Atmos. Sci.*, **51,** 2846–2866.

Gille, J. C., and J. M. Russell III, 1984: The Limb Infrared Monitor of the Stratosphere: Experiment description, performance and results. *J. Geophys. Res.*, **89,** 5125–5140.

Manney, G. L., and R. W. Zurek, 1993: Interhemispheric comparison of the development of the stratospheric polar vortex during fall: A 3-dimensional perspective for 1991–1992. *Geophys. Res. Lett.*, **20,** 1275–1278.

——, T. R. Nathan, and J. L. Stanford, 1988: Barotropic stability of realistic stratospheric jets. *J. Atmos. Sci.*, **45,** 2545–2555.

——, C. R. Mechoso, L. S. Elson, and J. D. Farrara, 1991a: Planetary scale waves in the Southern Hemisphere winter and early spring stratosphere: Stability analysis. *J. Atmos. Sci.*, **48,** 2509–2523.

——, J. D. Farrara, and C. R. Mechoso, 1991b: The behavior of wave 2 in the Southern Hemisphere stratosphere during late winter and early spring. *J. Atmos. Sci.*, **48,** 976–998.

Perliski, L. M., and J. London, 1989: Satellite observed long-term averaged seasonal and spatial ozone variations in the stratosphere. *Planet. Space Sci.* **37,** 1509–1525.

Randel, W. J., 1990: Kelvin wave–induced trace constituent oscillations in the equatorial stratosphere. *J. Geophys. Res.*, **95,** 18 641–18 652.

——, 1993: Global variations of zonal mean ozone during stratospheric warming events. *J. Atmos. Sci.*, **50,** 3308–3321.

——, and J. C. Gille, 1991: Kelvin wave variability in the upper stratosphere observed in SBUV ozone data. *J. Atmos. Sci.*, **48,** 2336–2349.

Reber, C. A., 1990: The Upper Atmosphere Research Satellite. *Eos, Trans. Amer. Geophys. Union,* **71,** 1867–1878.

Salby, M. L., 1982a: Sampling theory for asynoptic satellite observations. Part I: Space–time spectra, resolution and aliasing. *J. Atmos. Sci.*, **39,** 2577–2600.

——, 1982b: Sampling theory for asynoptic satellite observations. Part II: Fast Fourier synoptic mapping. *J. Atmos. Sci.*, **39,** 2601–2614.

——, P. Callaghan, S. Solomon, and R. R. Garcia, 1990: Chemical fluctuations associated with vertically propagating equatorial Kelvin waves. *J. Geophys. Res.*, **95,** 20 491–20 505.

Schäfer, J., 1979: A space–time analysis of tropospheric planetary waves in the Northern Hemisphere. *J. Atmos. Sci.*, **36,** 1117–1123.